

Optimization and Characterization of Bioactive Biocomposite Film Based on Orange Peel Incorporated With Gum Arabic Reinforced by Cr2O3 Nanoparticles

Saba Ghasemizad

Urmia University

Sajad Pirsā

Urmia University

Saber Amiri (✉ sa.amiri@urmia.ac.ir)

Urmia University <https://orcid.org/0000-0002-1176-4570>

Parisa Abdosatri

Urmia University

Research Article

Keywords: Biodegradable film, Orange peel, Gum Arabic, Cr2O3 nanoparticles, Response surface methodology

Posted Date: July 21st, 2021

DOI: <https://doi.org/10.21203/rs.3.rs-719348/v1>

License: © ⓘ This work is licensed under a Creative Commons Attribution 4.0 International License.

[Read Full License](#)

Version of Record: A version of this preprint was published at Journal of Polymers and the Environment on January 15th, 2022. See the published version at <https://doi.org/10.1007/s10924-021-02357-2>.

1 **Optimization and characterization of bioactive biocomposite film based on**
2 **orange peel incorporated with gum Arabic reinforced by Cr2O3**
3 **nanoparticles**

4
5 Saba Ghasemizad ¹, Sajad Pirsa ^{2*}, Saber Amiri ^{2**}, Parisa Abdosatri ²

6
7 ¹ Department of Food Science and Technology, Faculty of Agriculture, Saba Institute of
8 Higher Education, Urmia, Iran

9 ² Department of Food Science and Technology, Faculty of Agriculture, Urmia University,
10 P.O. Box 57561-51818, Urmia, Iran

11
12 Corresponding authors email: * pirsa7@gmail.com, s.pirsa@urmia.ac.ir

13 ** sa.amiri@urmia.ac.ir

26 **Abstract**

27 In this paper, the effect of adding gum Arabic at levels of 0-5%, and chromium oxide
28 nanoparticles (Cr_2O_3 NPs) at levels of 0-3%, are investigated on orange peel-based films. The
29 obtained results reveal a significant increase ($p < 0.05$) in water vapor permeability, weight
30 loss, tensile strength, and Young's modulus of film samples by increasing the percentage of
31 both gum and nanoparticles. Moreover, the addition of gum Arabic and Cr_2O_3 NPs decreases
32 the thickness, water-solubility, L^* , a^* , b^* indexes while increasing the elongation to the
33 breaking point. Furthermore, the moisture content of the film samples was decreased by the
34 addition of nanoparticles, however, the addition of gum Arabic increased this parameter. The
35 obtained results from the morphology of the samples indicated an increase in both roughness
36 and cracks by increasing the percentage of nanoparticles as well as creating a smooth surface
37 with the addition of gum Arabic. Besides, the results of FTIR revealed no new peak in the
38 prepared samples, as compared to the control sample. The results of XRD indicated that the
39 addition of gum Arabic and nanoparticles simultaneously caused the formation of new
40 crystals and increasing the crystallinity of the films. Based on TGA results, the thermal
41 stability of films containing the nanoparticles increased, as compared to the control sample.
42 In the meantime, the addition of gum and nanoparticles increased the antimicrobial properties
43 of the film samples, as compared to the control. Overall, those films created by the orange
44 peel including gum Arabic and Cr_2O_3 NPs could enhance the mechanical properties and
45 water vapor permeability of the samples.

46

47 **Keywords:** Biodegradable film; Orange peel; Gum Arabic; Cr_2O_3 nanoparticles; Response
48 surface methodology

49

50 **Introduction**

51 Plastic, well-known as one of the best human products, has now become a major challenge
52 for both the environment and humans since it is an indestructible material with a shelf life of
53 approximately 300 years. Here, it should be mentioned that the big volume of discarded
54 plastics resultant from the packaging of food and hygiene products, now has created several
55 problems, the most obvious of which is the irreparable damage to water, soil, air, and
56 creatures [1-3].

57 By increasing the population as well as pressure on the restricted resources and the
58 environment, the use of renewable resources to produce edible and biodegradable films has
59 become increasingly important, which can improve product quality or decrease the waste
60 disposal problems [4, 5]. Antimicrobial packaging as an active packaging type is one of the
61 packages, which has recently been widely used to increase the shelf life of food [6, 7].
62 Antimicrobial food packaging acts to inhibit or delay the growth of microorganisms possibly
63 existing in the food package or the packaged food. Metal oxide nanoparticles are among the
64 compounds used in the antimicrobial packaging, among which, special attention has been
65 paid to the formation and properties of chromium (Cr_2O_3), as an important heterogeneous
66 coating material, abrasion-resistant catalyst, solar energy storage, and high coloring .

67 Gums are one of the natural polymers that are recently utilized to synthesize the packaging
68 materials. Gums or hydrocolloids have been used since 5000 years ago [8, 9]. They are
69 generally consumed in the food industry to change the texture, rheological properties and
70 preserve the appearance of food as a result of their ability to stabilize emulsions and water
71 storage [10]. Gum Arabic is one of the types of hydrocolloids, which is the best type of gum
72 because of its emulsification and encapsulation properties for use in oil-in-water emulsion
73 systems [11]. Other advantages of gum Arabic include its cost-effectiveness, high
74 concentration, and widespread use of various products [12].

75 Orange fruit is widely used around the world as fresh produce and juice. Its peel is often
76 discarded as waste, which includes various secondary compounds with significant antioxidant
77 properties, as compared to other parts of the fruit [13]. Moreover, the orange peel is a good
78 source of molasses, pectin, and limonene, which are usually dried and mixed with dried pulp
79 and sold as animal feed [14]. In this paper, the orange peel powder was used as another
80 component to prepare the packaging film. For this purpose, the biodegradable film based on
81 orange peel incorporated with gum Arabic containing chromium oxide nanoparticles (Cr_2O_3
82 NPs) was optimized and characterized.

83

84 **Materials and methods**

85 **Materials**

86 The oranges (Valencia cultivar) were bought from the local market of Urmia, Iran. Gum
87 Arabic, Cr_2O_3 NPs, corn starch, glycerol, calcium nitrate, calcium sulfate, potassium sulfate,
88 sodium hydroxide, sodium chloride, and methanol 99.8% were from Merck (Darmstadt,
89 Germany). 2,2-diphenyl-1-picrylhydrazyl (DPPH) was made by Sigma-Aldrich (St. Louis,
90 MO, USA). The Nutrient agar culture medium was prepared by the Merck (Darmstadt,
91 Germany). Moreover, the standard strains of *Staphylococcus aureus* ATCC 25923 and
92 *Escherichia coli* H₇:O₁₅₇ ATCC 700728 were prepared from the Iran Industrial and Scientific
93 Research Organization, Tehran, Iran.

94 **Preparing orange peel powder (OPP)**

95 The orange peel was dried at room temperature after washing and ground. After sieving, the
96 resulting powder was covered in a plastic bag and was stored in the refrigerator .

97 **Film preparation**

98 At first, two grams of orange peel were dissolved in 100 ml of distilled water and then stirred
99 for 20 h on a heated mixer at 30 °C at 250 RPM. Then, after 20 h, 40% glycerol (based on the

100 dry weight of orange peel) was added and stirred again for 30 min. In the end, after filtration,
101 the prepared solution was poured into 35 ml plates and then dried at room temperature .

102 **Film characteristics**

103 **Thickness**

104 The film thickness was measured using a digital micrometer at five random points of each
105 film (around and center of each film). Afterward, the average thickness of different points of
106 each film was utilized to calculate the mechanical properties and water vapor permeability
107 [15].

108 **Weight loss percentage**

109 To measure the weight loss of the films, small pieces of the film were dried in an oven at 105
110 °C for 24 h. Then, the weight of the films was recorded before and after drying in the oven.
111 The amount of weight loss was then calculated as the percentage of initial weight loss as
112 follows :

$$113 \text{ Weight loss} = \frac{(W_0 - W)}{W_0}$$

114 where W_0 means the initial dry weight, W_1 represents the final dry weight [16] .

115 **Measuring the moisture content of the films**

116 The films were cut into 2×2 cm and then weighed carefully. Afterward, they were placed in
117 aluminum dishes and dried in an oven at 105 °C for 24 h. The moisture content was
118 calculated based on the difference between the initial and final weight of the samples [17].

119 **Water solubility**

120 To measure the water solubility of the films, the film samples were prepared in 2×2 cm. They
121 were placed in an oven at 110 °C for 6 h to obtain the initial dry weight. After weighing (W_1),
122 the samples were immersed in the sealed dishes containing 50 ml of distilled water. The
123 dishes were stirred as cross-sectional at 25 °C for 18 h. Then, the films were removed from
124 the water and again placed in an oven at 110 °C for 6 h to achieve a constant weight. By re-

125 weighing, the samples, the final dry weight (W_2) was obtained. The percentage of water
126 solubility was calculated as follows [18]:

127
$$\%WS = \frac{W_1 - W_2}{W_1} \times 100$$

128 where W_1 is the initial dry weight and W_2 denotes the final dry weight .

129 **Measuring water vapor permeability (WVP)**

130 ASTM E96-05 method is employed to measure water vapor transfer (ASTM, 2005) using the
131 special vials. There was a 5 mm diameter hole in the lid of these vials, in which a piece of
132 film was placed. Then, 3 g of calcium sulfate was placed in vials. A piece of film was cut and
133 then placed in the lid of the vial, and closed on the vial. The vials were weighed with all the
134 contents and then placed in a desiccator containing a saturated solution of potassium sulfate.
135 To ensure saturation, some precipitate of potassium sulfate was allowed to form on the
136 bottom of the desiccator . Saturated potassium sulfate at 25 °C produces a relative humidity
137 of 97%. Then, the weight of the vials was measured every 4 days for several hours.

138 The amount of water vapor transferred from the films was determined by increasing the
139 weight of the vials. The weight gain curve of the vials over time was plotted, and after
140 calculating the linear regression, the slope of the resulting line was calculated. Dividing the
141 slope of the line associated with each vial by the total surface area of the film exposed to
142 water vapor transfer, the water vapor transfer rate (WVTR) is obtained. The water vapor
143 permeability (WVP) was then calculated as follows :

144
$$WVP = \frac{WVTR}{P(R_1 - R_2)} \cdot X$$

145 where X means the film thickness (m), P denotes the pure water vapor pressure at 25 °C
146 (3169 Pa), R_1 refers to the relative moisture in the desiccator (97%), and R_2 is the relative
147 moisture inside the vial (0 %). The test was implemented on each sample in three repetitions .

148 **Measuring color properties**

149 A colorimetric device was employed to specify the surface color of the film samples. The
150 results were exhibited in light-dark (L^*), green-red (a^*), and blue-yellow (b^*) [19]. Besides,
151 the whiteness index (WI) and Chroma (C^*) were calculated using the following equations :

$$152 \quad WI = 100 - \sqrt{(100 - L^*)^2 + a^{*2} + b^{*2}}$$

$$153 \quad Chroma = \sqrt{(a^*)^2 + (b^*)^2}$$

154

155 **Measuring mechanical properties**

156 The mechanical properties of the film samples were specified using the tensile tests by a
157 Texture Analyzer based on the instructions of the ASTM D882-10 standard method. To
158 implement the tensile test, the samples were conditioned in a desiccator including the
159 magnesium nitrate saturated solution with relative moisture of $50 \pm 5\%$ for 24 h. Then, they
160 were cut into rectangular strips, and both longitudinal ends of each film were placed between
161 the two jaws of the device [20]. By initiating the test operation, the film was pulled between
162 the two jaws until it was torn, based on which the work process appeared as a stress-strain
163 diagram. The tensile strength, elongation at the breaking point, and the modulus of elasticity
164 properties of the films were calculated as follows :

$$165 \quad \text{Ultimate tensile strength} = \frac{F_{\max}}{A}$$

$$166 \quad \text{Elongation at break} = \frac{L_{\max}}{L_0} \times 100$$

$$167 \quad \text{Young's modulus} = \frac{(F \cdot L_0)}{(A \cdot \Delta L)}$$

168 where A represents the film cross-sectional area (m^2), F_{\max} denotes the maximum force at the
169 breakpoint (N), L_{\max} means the film elongation at the breakpoint (m), L_0 is the initial length
170 of film sample (m), F is the force (N) and ΔL represents the changes in the length of the
171 sample to the breaking point (m).

172 **Field emission scanning electron microscopy (FE-SEM)**

173 To evaluate the morphology, the surface of the film samples was examined using Field
174 emission scanning electron microscopy (FE-SEM) at room temperature. Before scanning, a
175 gold coating in several nanometers thickness was coated on the fracture surfaces [21].

176 **Fourier transform infrared spectroscopy (FTIR) test**

177 Fourier transform infrared spectroscopy (FTIR) was utilized in the range of 400-4000 cm^{-1} to
178 survey the interactions in the film matrix. First, the device was zeroed with KBr tablet as a
179 control sample, and then the samples were prepared for FT-IR analysis by mixing 1 mg of
180 completely dried samples via 150 mg of dry KBr powder. The thin tablets were prepared
181 from each sample by compressing the mixture in a press device [22].

182 **X-ray diffraction test (XRD)**

183 X-ray diffraction pattern of the film samples was employed to investigate the crystal structure
184 of the prepared films and determine the distribution of components in the polymer matrix
185 [23].

186 **Thermogravimetric analysis (TGA) change test**

187 The dried film samples were analyzed from 20 to 500 $^{\circ}\text{C}$ at a heating rate of 10 $^{\circ}\text{C}/\text{min}$ along
188 with the pure nitrogen gas at a rate of 20 mm/min .

189 **Investigating antimicrobial properties of the films**

190 To determine the antimicrobial properties of active films, the method of penetration of
191 antimicrobial compounds in agar medium (every 4 days) was utilized. In this method, the
192 films were cut into circular plates and then transferred to the nutrient agar culture medium,
193 which was previously inoculated with 10^5 - 10^6 cfu/ml of *Escherichia coli* (*E. coli*) or
194 *Staphylococcus aureus* (*S. aureus*) microorganisms. After that, petri dishes comprising the
195 contaminated culture medium along with antimicrobial films were kept in an incubator at 37
196 $^{\circ}\text{C}$ for 24 h. To obtain the degree of the microorganisms growth inhibition by the film, the

197 diameter of the growth inhibition zone formed around the films was measured using a caliper
198 [24].

199 **Statistical analysis**

200 In this paper, the effect of two numerical factors on the concentration of gum Arabic and
201 Cr₂O₃ NPs are investigated using the Response Surface Methodology (RSM) in the form of a
202 central composite design. In this design, 13 samples (including 4 factorial points, 4 axial
203 points, and 5 central points are considered to estimate the mismatching and reproducibility).
204 After implementing the experiments and data collection to test the significance of the factors
205 and their interactions, the method of analysis of variance (ANOVA) and Fisher distribution
206 was employed at the significance level of $\alpha=0.05$. The Design expert software V.11 was
207 utilized to analyze the data and draw the graphs .

208

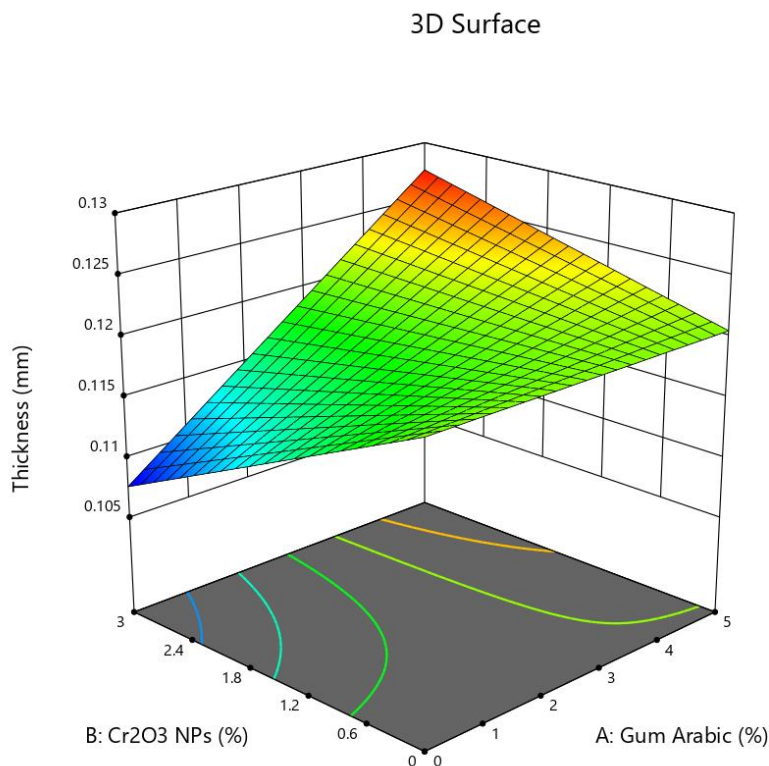
209 **Results and discussion**

210 **Thickness**

211 The results indicated that by increasing the percentage of Cr₂O₃ NPs, the film thickness
212 decreased, whereas the addition of gum Arabic had little effect on the film sample thickness
213 (Fig. 1). Overall, those films via the highest levels of nanoparticles and gum had the highest
214 thickness, which might be due to the increase in the solid materials [25]. The reason for the
215 thickness reduction behavior through increasing the nanoparticle percentage is also related to
216 the increased density in the polymer film structure by the Cr₂O₃ NPs. According to the results
217 of several researchers, it can be concluded that the thickness of the films changes based on
218 the type of polymer and the added nanoparticles, and can cause the thickness to decrease,
219 increase, or remain constant .

Factor Coding: Actual

Thickness (mm)
Thic (mm)
0.108 0.128
X1 = A: Gum Arabic
X2 = B: Cr2O3 NPs
X1 = A: Gum Arabic
X2 = B: Cr2O3 NPs



220
221

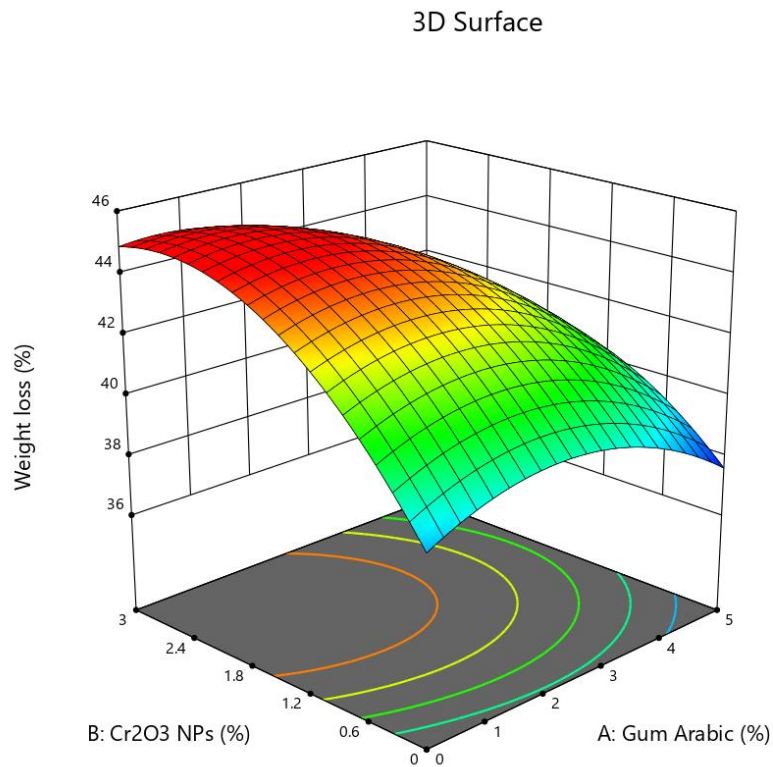
222 **Fig. 1:** The three-dimensional curve of the effect of nanoparticle-gum percentage on the
223 thickness of films

224

225 Weight loss

226 Fig. 2 illustrates the three-dimensional curve of the film weight loss percentage. By
227 increasing the gum content percentage, the film weight loss percentage reduced while
228 increasing the Cr₂O₃ NPs, it was increased significantly (p<0.05). It should be noted that
229 those samples containing the highest levels of nanoparticles and no gum Arabic had the
230 highest weight loss. Moreover, the effect of the second-degree percentage of gum and Cr₂O₃
231 NPs on weight loss was also significant .

Factor Coding: Actual
 Weight loss (%)
 37.5 44.91
 X1 = A: Gum Arabic
 X2 = B: Cr2O3 NPs
 X1 = A: Gum Arabic
 X2 = B: Cr2O3 NPs



232
 233

234 **Fig. 2:** The three-dimensional curve of the effect of nanoparticle-gum percentage on the
 235 percentage of weight loss of films

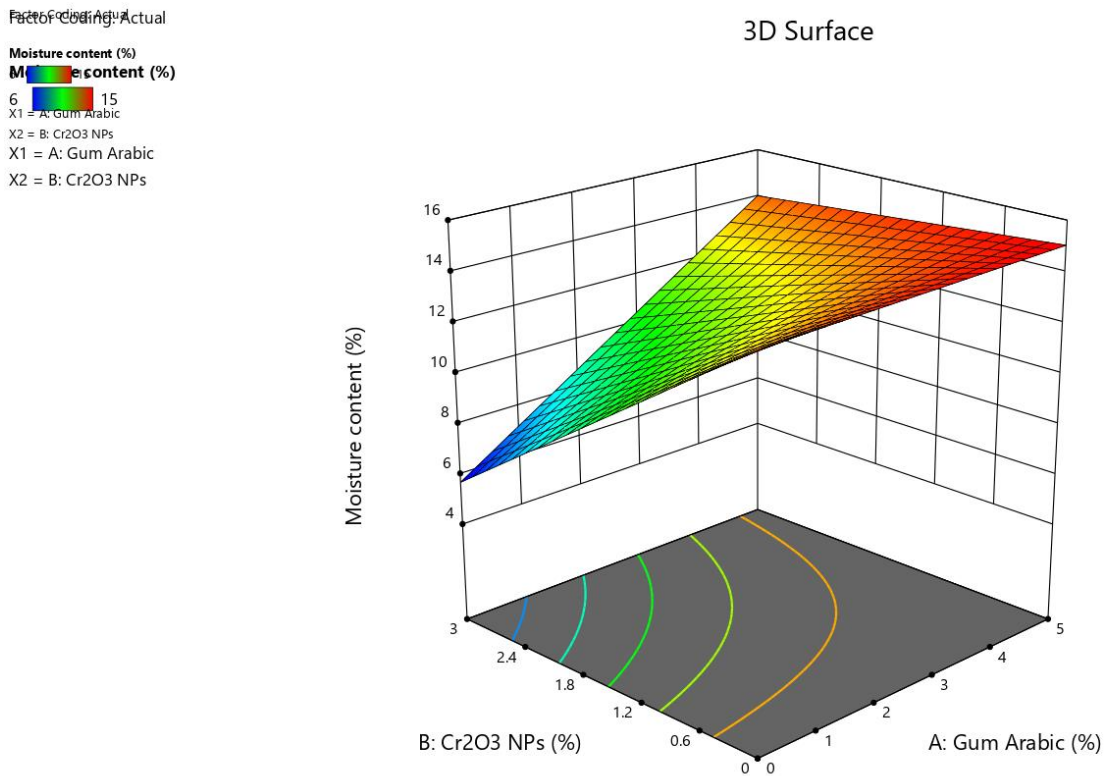
236

237 **Measuring the moisture content of the films**

238 Fig. 3 depicts the three-dimensional curve of the effect of gum and Cr₂O₃ NPs percentage on
 239 the amount of moisture. It should be mentioned that by increasing the percentage of gum, the
 240 moisture content of the film increased, while by increasing the percentage of Cr₂O₃ NPs, the
 241 moisture content of the film significantly decreased (p<0.05).

242 Besides, the moisture content of the film increased by increasing the gum. This seems to be
 243 due to the increased compression of the film matrix and the entrapment of more water in the
 244 film matrix structure. On the other hand, high hydrophilicity of the gum cause more water
 245 absorption by the gum and thus increasing the moisture content of the films [26].
 246 Furthermore, the reduction in the moisture content with the addition of nanoparticles is likely

247 due to the weak interaction of nanoparticles with the hydroxyl polymer group [25]. Our
248 results in terms of the effect of adding nanoparticles on reducing the moisture content of
249 films are in accordance with the results of Li et al. [27] who added zinc oxide nanoparticles to
250 chitosan, as well as Bahrami et al. [25] adding the silver nanoparticles to the films based on
251 hydroxypropyl methylcellulose and Tragacanth.



252
253

254 **Fig. 3:** The three-dimensional curve of the effect of nanoparticle-gum percentage on the
255 moisture content of the films

256

257 **Water solubility**

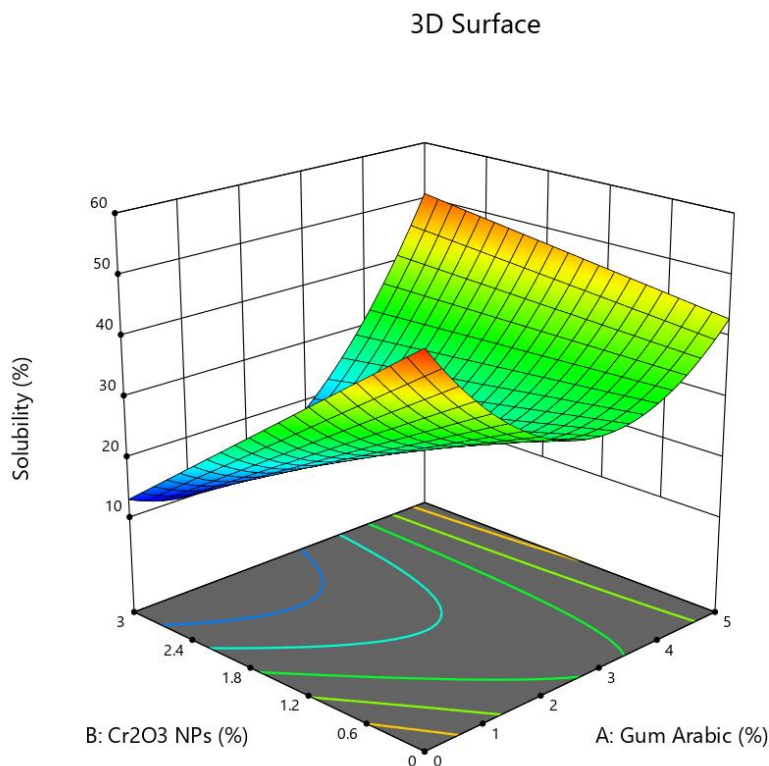
258 Fig. 4 exhibits the three-dimensional curve of the film solubility as a function of two
259 variables of the gum and Cr₂O₃ NPs percentages. The obtained results revealed that by
260 increasing the percentage of gum and Cr₂O₃ NPs, the solubility of the film decreased. Note

261 that the second-degree effect of gum and the linear effect of Cr₂O₃ NPs were also
262 significant .

263 Here, it is worth noting that solubility is an essential feature in biodegradable films because it
264 can resist the film compared to water, especially in the environment containing moisture such
265 as meat products, and determine the release speed of antioxidant and antimicrobial
266 compounds when in contact with the material food. Adding the nanoparticles increases the
267 electrostatic bonding between film polymer, and thus decreasing the water solubility of the
268 film. Some similar results are provided by adding clay nanoparticles to the film based on
269 pectin [28]. Rezaei et al. [29] reported that the addition of zinc oxide nanoparticles reduced
270 the water solubility of the films . Our results in terms of the effect of gum on reducing water
271 solubility were in accordance with the result of Sui et al. [30]. They found reduced water
272 solubility by increasing the amount of Tragacanth. Khoirunnisa et al. [31] expressed that the
273 addition of zinc nanoxide led to a significant change in the solubility of the films, which was
274 consistent with our findings in terms of the effect of nanoparticles on reducing the water
275 solubility of film.

276 They described this phenomenon attributed to the possible bonding between nanoparticles
277 and film matrix. Some studies revealed that the addition of nanoparticles causes hydrogen
278 bonding between nanoparticles and polymer matrix. As such, the bonding of free molecules
279 of water and hydrophilic biopolymer groups reduced, and subsequently, the film solubility
280 decreased [32].

Factor Coding: Actual
 Solubility (%)
 Soft (%)
 12.05 55.2
 X1 = A: Gum Arabic
 X2 = B: Cr2O3 NPs
 X1 = A: Gum Arabic
 X2 = B: Cr2O3 NPs



281
 282

283 **Fig. 4:** A three-dimensional curve of the percentage of nanoparticle-gum on the water
 284 solubility of films

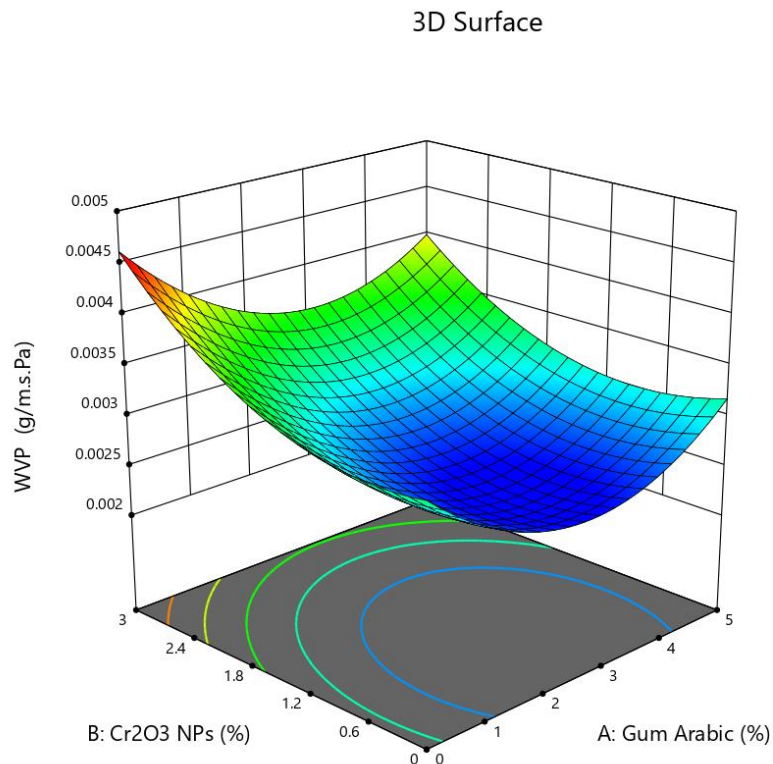
285

286 **Measurement of water vapor permeability (WVP)**

287 Fig.5 illustrates the three-dimensional curve of water vapor permeability (WVP) as a function
 288 of two variables of gum and Cr₂O₃ NPs. The results of the statistical analysis confirmed that
 289 by increasing Cr₂O₃ NPs, the amount of WVP increases significantly. Moreover, by
 290 increasing the gum surfaces, the amount of WVP of the samples decreased, and then slightly
 291 increased.

292 Furthermore, the second-degree effect of gum and Cr₂O₃ NPs was significant on WVP
 293 (p<0.05). Note that increasing the WVP of the films by adding nanoparticles, is due to porous
 294 structure and gaps caused by nanoparticles [33]. Similar results were obtained for films
 295 comprising Gracilaria vermiculophylla extract and zinc oxide nanoparticles [33].

Factor Coding: Actual
 WVP (g/m.s.Pa)
 WVP (g/m.s.Pa)
 0.0025 0.0045
 X1 = A: Gum Arabic
 X2 = B: Cr2O3 NPs
 X1 = A: Gum Arabic
 X2 = B: Cr2O3 NPs



296
 297

298 **Fig. 5:** A three-dimensional curve of the percentage of nanoparticle-gum on the water vapor
 299 permeability of the films

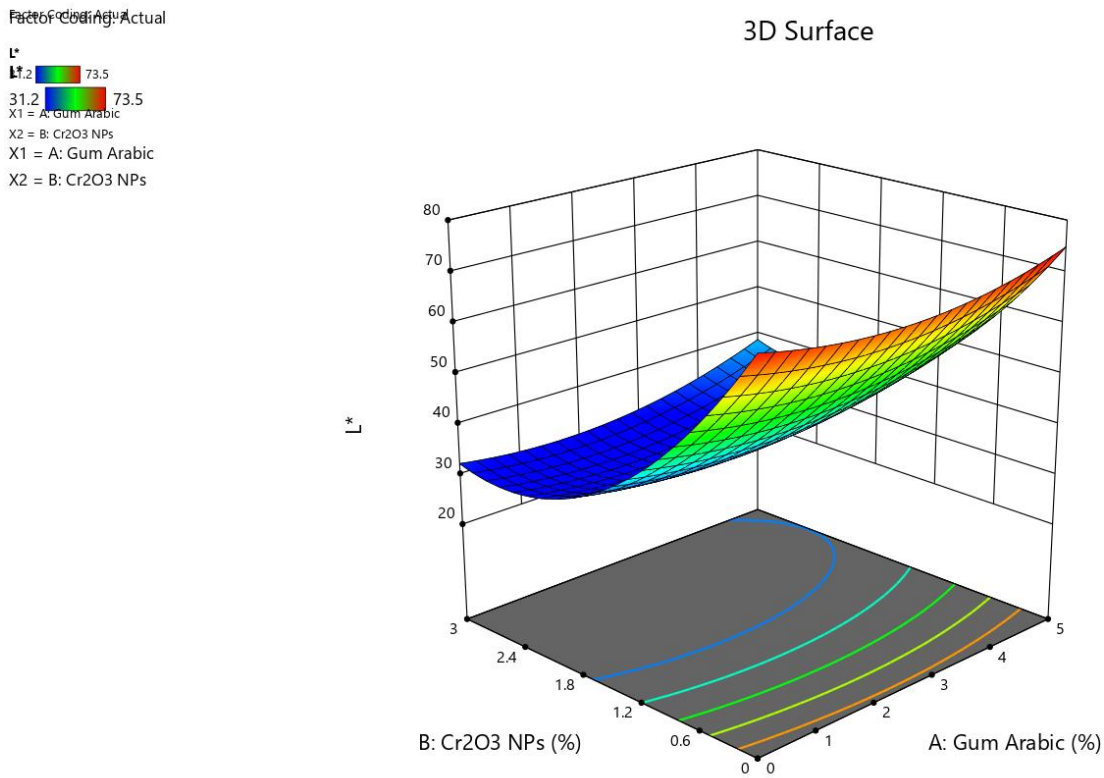
300

301 Measuring color properties

302 The color and appearance of the polymer used in food packaging is an essential and effective
 303 factor for choosing and accepting the product by the consumer. Most food packaging films
 304 are transparent and colorless. Nevertheless, in some cases, the use of the inhibitor compounds
 305 of light, and generating the color in the matrix of the packaging material are necessary, due to
 306 the sensitivity of food to light, the loss of its nutritional compounds by optical oxidation, and
 307 color matching contents with packaging material to attract the consumer attention [34].

308 Fig. 6 depicts the three-dimensional curve of film lightness (L^*) as a function of two
 309 variables of gum and Cr_2O_3 NPs percentages. The obtained results of the statistical analysis

310 revealed that by increasing the gum percentage, the film L^* increased; however, by
 311 increasing the percentage of Cr_2O_3 NPs, the amount of the film L^* decreases significantly .
 312 Sui et al. [30] indicated that the higher the ratio of gum to soy protein isolate, the brighter the
 313 color of the film will be. This is in line with our results revealing the increased L^* along with
 314 increasing the gum. As can be observed, by increasing nanoparticles, the transparency of the
 315 films decreases, which was in accordance with the results of Asdagh et al. [35]. They
 316 described that by increasing the number of nanofibers, the transparency of polylactic acid
 317 films decreased. Besides, the decrease in L^* with the addition of nanoparticles may be due to
 318 the matte appearance of Cr_2O_3 NPs [25].

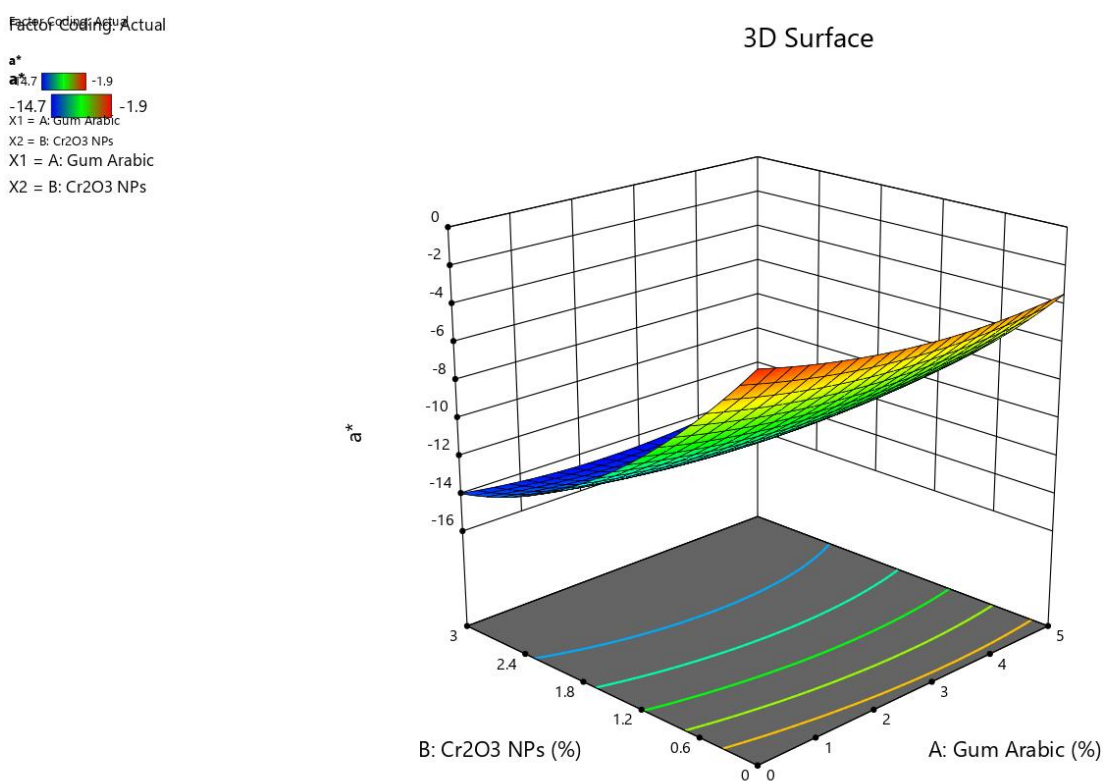


319
 320

321 **Fig. 6:** A three-dimensional curve of the percentage of nanoparticle-gum on the L^* index
 322 of films

323

324 Fig. 7 exhibits the three-dimensional curve of the a^* index of the film as a function of two
 325 variables of gum and Cr_2O_3 NPs. The results indicated that by increasing the gum percentage,
 326 the value of a^* index increased, while by increasing the Cr_2O_3 NPs, the a^* index content of
 327 the films decreased.
 328 In terms of the effect of nanoparticles, it could be seen that by adding nanoparticles, the value
 329 of a^* was reduced, which was consistent with the results of Oleyaei et al. [26].
 330



331
 332 **Fig. 7:** A three-dimensional curve of the percentage of nanoparticle-gum on the parameter
 333 a^* index films

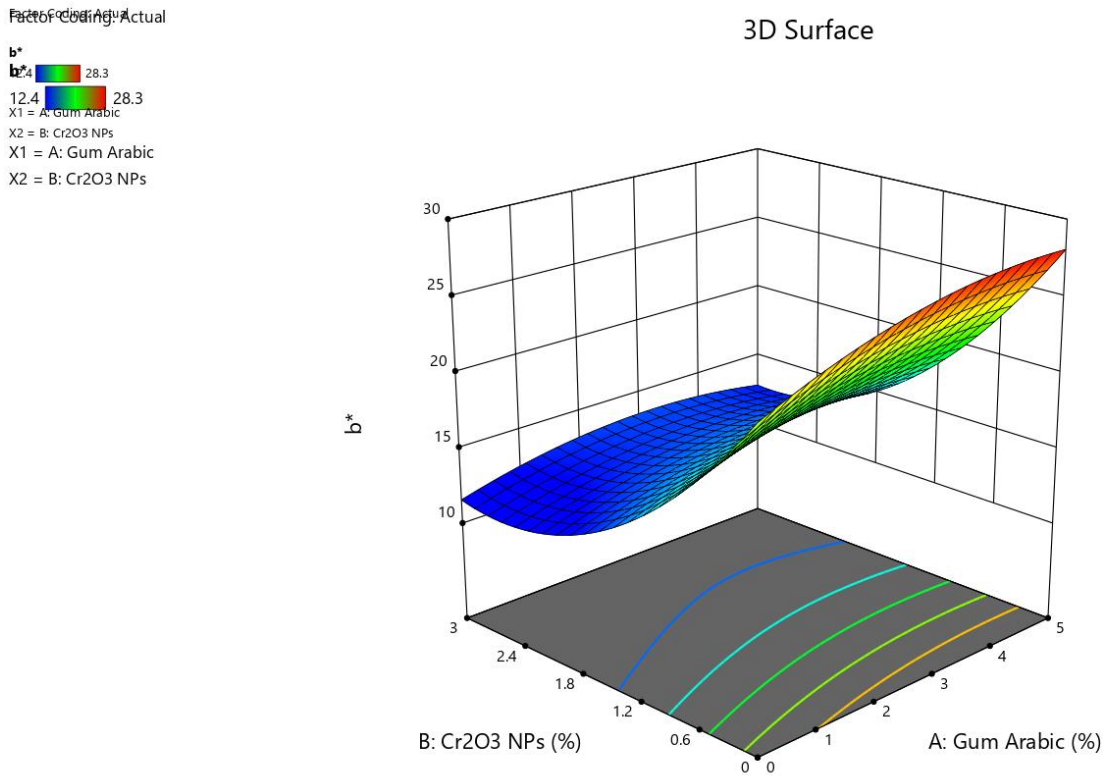
334
 335 Fig. 8 illustrates the three-dimensional curve of the b^* index of the film as a function of
 336 two variables of gum and Cr_2O_3 NPs. The results of statistical analysis indicated that by
 337 increasing the percentage of gum, the amount of b^* index of the film increased, while by

338 increasing the percentage of Cr₂O₃ NPs, the b* index of the film significantly decreased.

339 Considering the effect of nanoparticles, it can be observed that by the addition of

340 nanoparticles, the b* was decreased, which was in line with the results of Oleyaei et al. [26].

341



342

343 **Fig. 8:** A three-dimensional curve of the percentage of nanoparticle-gum on the parameter

344 b* index films

345

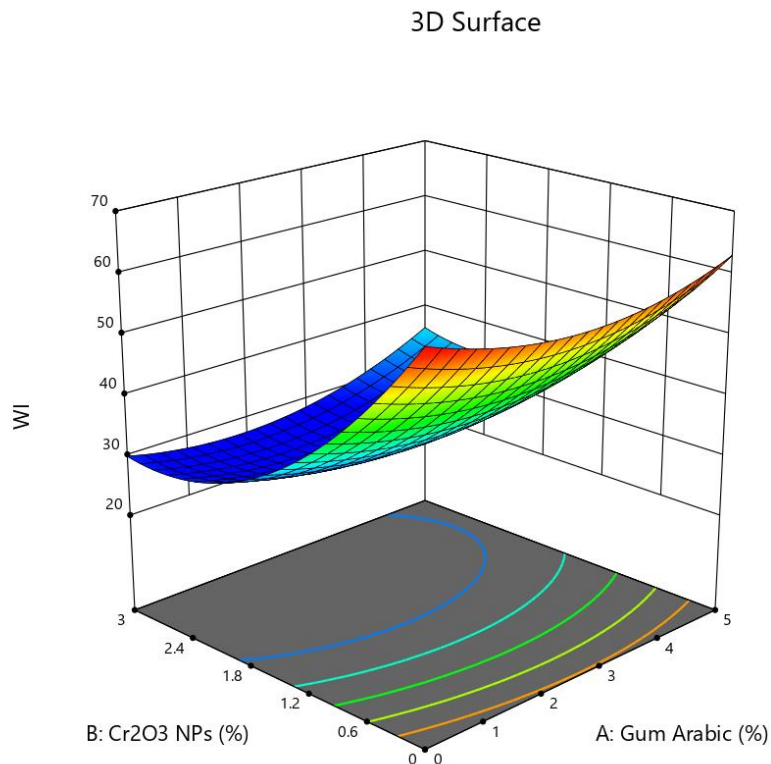
346 Fig. 9 depicts a three-dimensional whiteness index (WI) as a function of two variables of

347 gum and Cr₂O₃ NPs percentage. The obtained results confirmed that the WI rate increased by

348 increasing the percentage of gum, whereas by increasing the Cr₂O₃ NPs, the WI decreased .

349

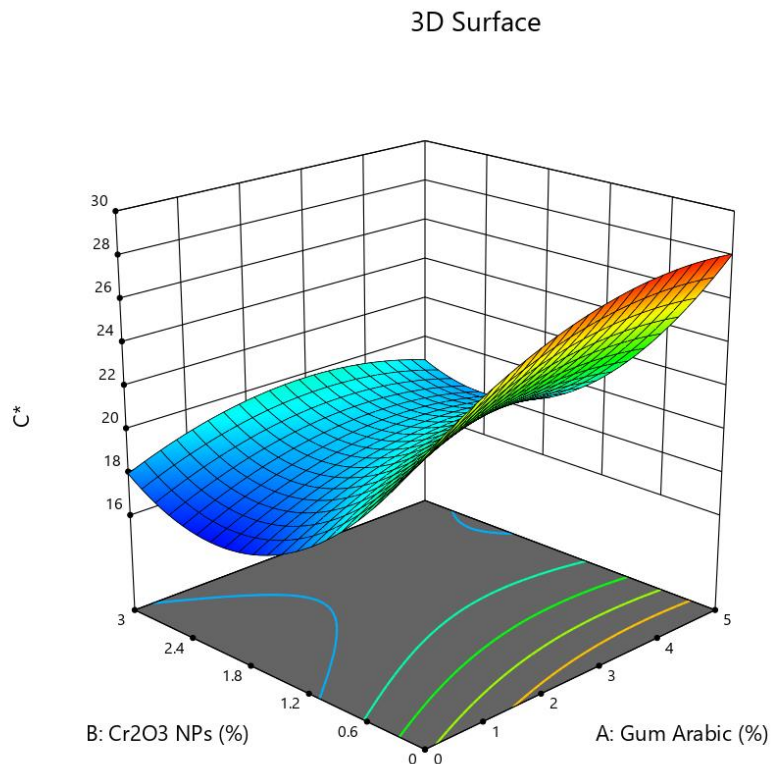
Factor Coding: Actual
 WI
 28.8218 62.7804
 X1 = A: Gum Arabic
 X2 = B: Cr2O3 NPs
 X1 = A: Gum Arabic
 X2 = B: Cr2O3 NPs



350
 351 **Fig. 9:** A three-dimensional curve for the effect of the percentage of nanoparticle-gum on the
 352
 353
 354
 355
 356
 357
 358
 359
 360
 361
 362

Fig. 10 exhibits the three-dimensional curve of the film as a function of two variables of gum and Cr₂O₃ NPs percentage. The statistical analysis revealed that by increasing the gum percentage, the amount of C* index in the film increased, while by increasing the percentage of Cr₂O₃ NPs, the film C* significantly decreased (p<0.05). The C* denotes a measure of a color difference of gray, which can be defined as color purity. The calculation of the amount of C* in the samples shows the highest amount of purity in the film samples. The results in this regard were consistent with the results of He et al. [36]. They provided that with the addition of oxide nanoparticles, the amount of C* decreased.

Factor Coding: Actual
 C*
 16.2265 28.554
 X1 = A: Gum Arabic
 X2 = B: Cr2O3 NPs
 X1 = A: Gum Arabic
 X2 = B: Cr2O3 NPs



363
 364 **Fig. 10:** The three-dimensional curve of the nanoparticle-gum percentage on C* index of
 365 films

366
 367 **Measuring mechanical properties**

368 Mechanical properties are considered the most important properties of materials used in food
 369 packaging. Among the important mechanical properties of biodegradable films are the tensile
 370 strength and tensilability to the breaking point to determine their resistances in different
 371 processes, transportation, and warehousing .

372 Table 1 lists the percentage of elongation, tensile strength, and elastic modulus of samples 6,
 373 8, 12 against the control sample (sample 13). As can be observed, by adding the gum Arabic
 374 and nanoparticles in samples 6 and 12, the tensile resistance parameter has a significant
 375 increase, as compared to the control sample. This can be associated with the creation of
 376 appropriate interactions between film matrix and additive materials (such as gum Arabic and
 377 Cr₂O₃ NPs), where this parameter increased by forming new hydrogen bonding.

378 Furthermore, the uniformity of nanoparticles in the films increases the tensile strength, as
 379 compared to the control sample [37]. Moreover, the modulus of the elasticity reveals the
 380 same process and indicates the creation of interactions in the film matrix. This is in line with
 381 the results of Xu et al. [11] in terms of the addition of the ZnO-CMC combined nanoparticles
 382 to the pea starch film. Besides, He et al. [36] proposed that two parameters of elasticity
 383 modulus and tensile strength were increased by adding the zinc nanoxide to the gelatin fish .
 384 In this matter, the addition of titanium oxide and silver nanoparticles to the Carboxymethyl
 385 cellulose film increased both the tensile strength and modulus of elasticity [37]. However, in
 386 sample 8 (i.e. the sample including the highest percentage of gum Arabic and chromium
 387 oxide), it can be seen the decrease in these two parameters can be associated with the lack of
 388 adequate interactions with the film matrix and the formation of bonding between
 389 nanoparticles and gum. In other words, instead of the formation of abundant hydrogen
 390 bonding with film matrix, nanoparticles and gum create abundant hydrogen bonding with
 391 each other, which finally would result in reducing the tensile strength elasticity modulus.
 392 Meanwhile, there was no logical process for the percentage of elongation (% E).

393 **Table 1:** The data on the mechanical properties of films based on orange peel and gum

394

Sample	% E	YM (MPa)	TS (MPa)
OPP	$\pm 0.88^b$ 21.62	34.07 ± 1.21^a	7.34 ± 0.10^a
OPP /AG	17.69 ± 0.67^a	60.41 ± 4.36^c	10.63 ± 0.39^c
OPP /Cr ₂ O ₃	$\pm 0.13^b$ 21.29	50.54 ± 0.73^b	10.76 ± 0.18^c
OPP /Cr ₂ O ₃ /AG	$\pm 0.83^b$ 20.95	41.98 ± 2.10^a	8.76 ± 0.20^b

395 Different letters in each column indicate significance at the level of $p < 0.05$.

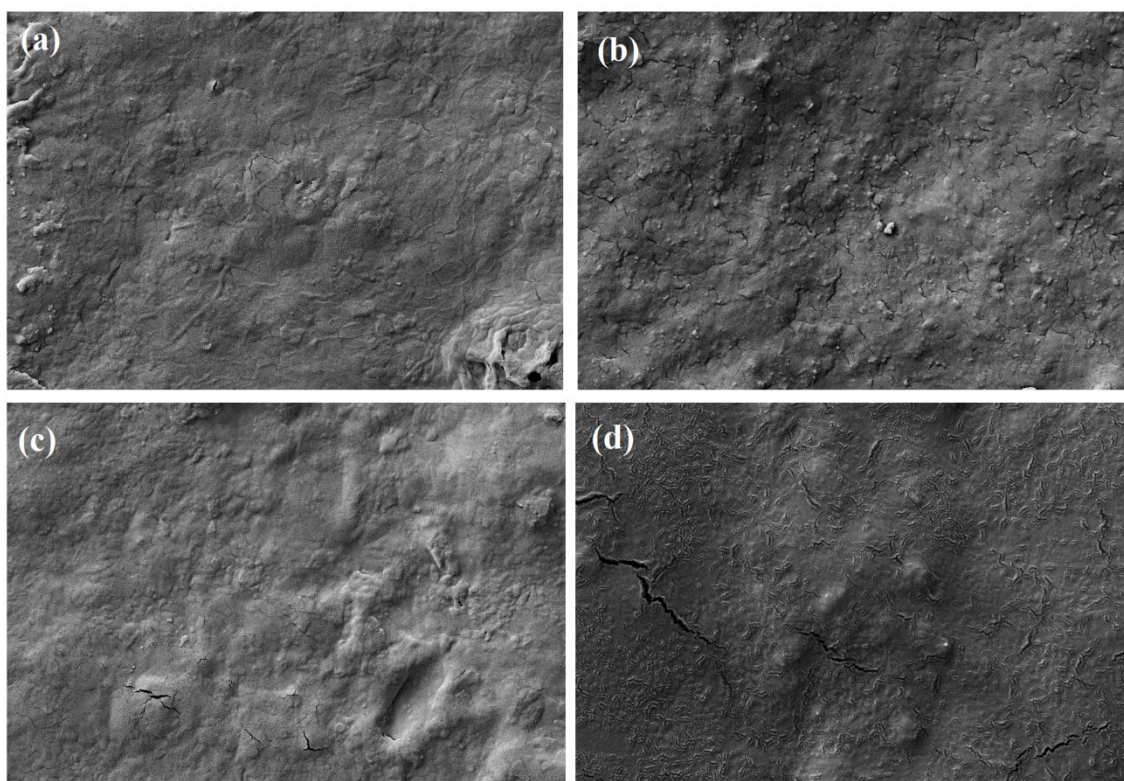
396

397 **Field emission scanning electron microscopy (FE-SEM)**

398 The analysis of the film's morphology provides information on the spatial layout of different
399 components in the film, which helps understand the mechanical properties and water vapor
400 transfer mechanisms [38]. In this regard, the SEM images resulting from the sample surface
401 of the films are depicted in Fig. 11. The SEM images show the control film based on the
402 dense and uniform surface of orange peel (Fig. 11a). As can be observed from Fig. 11b,
403 Cr_2O_3 NPs were uniformly distributed without agglomeration of particles at the surface of the
404 film sample. Besides, as compared to the control sample, adding nanoparticles to films
405 caused rough surfaces, more cracks, and a break at the surface of the film samples .

406 Oun and Rhim [39] reported the uniform distribution of zinc oxide nanoparticles in
407 carrageenan films. Based on Fig. 11c, the addition of gum Arabic to orange peel films caused
408 a uniform surface with no fracture. This condition may be resultant due to intra-molecular
409 interaction between polymer matrix. In this regard, the results of coordination were achieved
410 for those films based on carrageenan gum, Xanthan Gum, and Gellan gum, which were
411 prepared with different proportions [40].

412 In the images related to films containing 5% gum and 3% of Cr_2O_3 NPs, surface with more
413 and deeper cracks and fractures, and more non-uniformity can be seen, as compared to the
414 control sample. Besides, they had a non-homogeneous surface than the control film (Fig.
415 11d). These results are probably due to the interaction between polymer, gum, and
416 nanoparticles. Martins et al. [41] reported that films based on the carrageenan and lacuste
417 gum had a uniform and dense surface and the addition of clay nanoparticles increased the
418 roughness of the samples. Moreover, the addition of TiO_2 nanoparticles to films based on
419 carrageenan gum, Xanthan Gum, and Gellan gum, caused the roughness of the sample [40].



420

421 **Fig. 11:** The field emission scanning electron microscopy images (a) OPP, (b) OPP / Cr₂O₃,

422 (c) OPP / AG, and (d) OPP / Cr₂O₃ / AG

423

424 **Fourier transform infrared spectroscopy (FTIR) test**

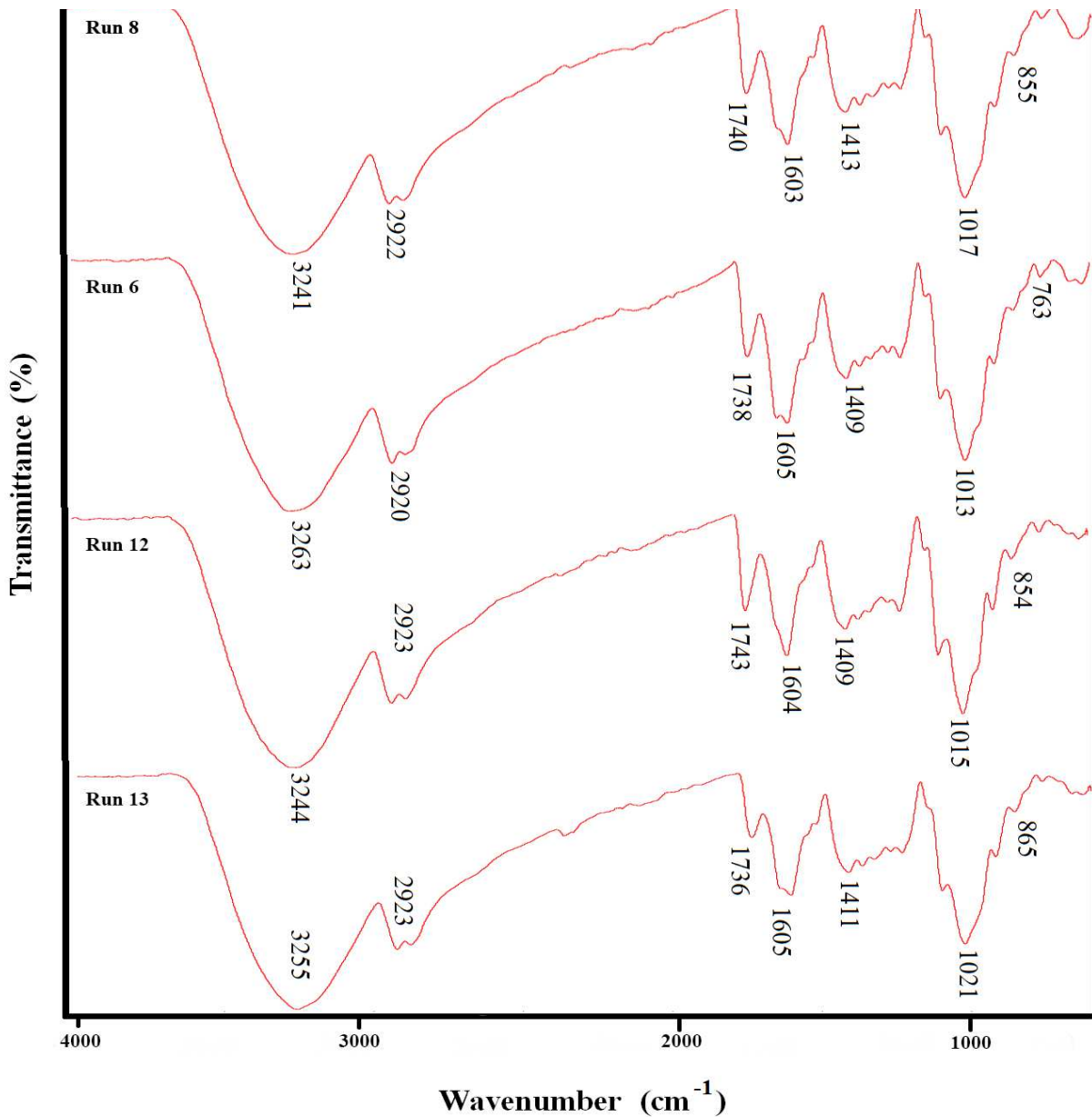
425 FTIR analysis is a useful and practical method to study and identify the intra-molecular
 426 interactions of the film samples. FTIR spectra of the film samples are provided in Fig. 12.

427 The peaks of the film are in the range of 600 cm⁻¹ to 4000 cm⁻¹. The FTIR spectra of the
 428 control films were almost similar to other film samples and there was no significant change in
 429 their functional groups. Meanwhile, there was no new peak in the film samples, indicating no
 430 change in the pectin-based film of the orange peel comprising gum Arabic and nanoparticles.

431 Overall, the position and severity of changed peaks are related to the interaction between
 432 nanoparticles and gum Arabic with a polymer matrix. The peak index in 325 cm⁻¹ reveals the

433 tensile vibrations of O-H and CH₂-OH groups, which is related to the presence of starch,
 434 glycerol, and water compounds. Besides, the peak at 2923 cm⁻¹ is related to the C-H

435 alkankins and compounds in the polymer film matrix [42]. In this way, the absorbed bands of
436 2870-2960 cm^{-1} are attributed to the symmetric and asymmetric C-H groups [42, 43]. The
437 peak in the range of 1605 cm^{-1} is related to the N-H Amide groups. Moreover, the absorption
438 band in 1740 cm^{-1} represents the presence of tensile bonding C=O in the Amide groups [44].
439 The absorption peak in the range of 1410 cm^{-1} is related to the vibrational group of O-H.
440 Meanwhile, the absorption peak in the range of 1200 cm^{-1} to 1350 cm^{-1} represents the
441 existence of the C-O tensile group in the Polysaccharide complex. The peak existing in the
442 range of 1015 cm^{-1} to 1950 cm^{-1} denotes C=O tensile and vibrating groups. Moreover, the
443 peaks observed in the range of 650 cm^{-1} to 950 cm^{-1} are related to the C=C and C-H bonding
444 of the aromatic ring [45]. Overall, the addition of gum Arabic and Cr_2O_3 NPs did not create a
445 new peak in the FTIR spectra.
446



447

448 **Fig. 12:** The FTIR spectroscopy (RUN 13) OPP, (RUN 6) OPP / Cr₂O₃, (RUN12) OPP / AG

449

and (RUN 8) OPP / Cr₂O₃ / AG

450

451 **X-ray diffraction test (XRD)**

452 The X-ray diffraction pattern is utilized to investigate the crystalline behavior of edible films

453 and their morphological properties [23]. The structure of compound films containing gum

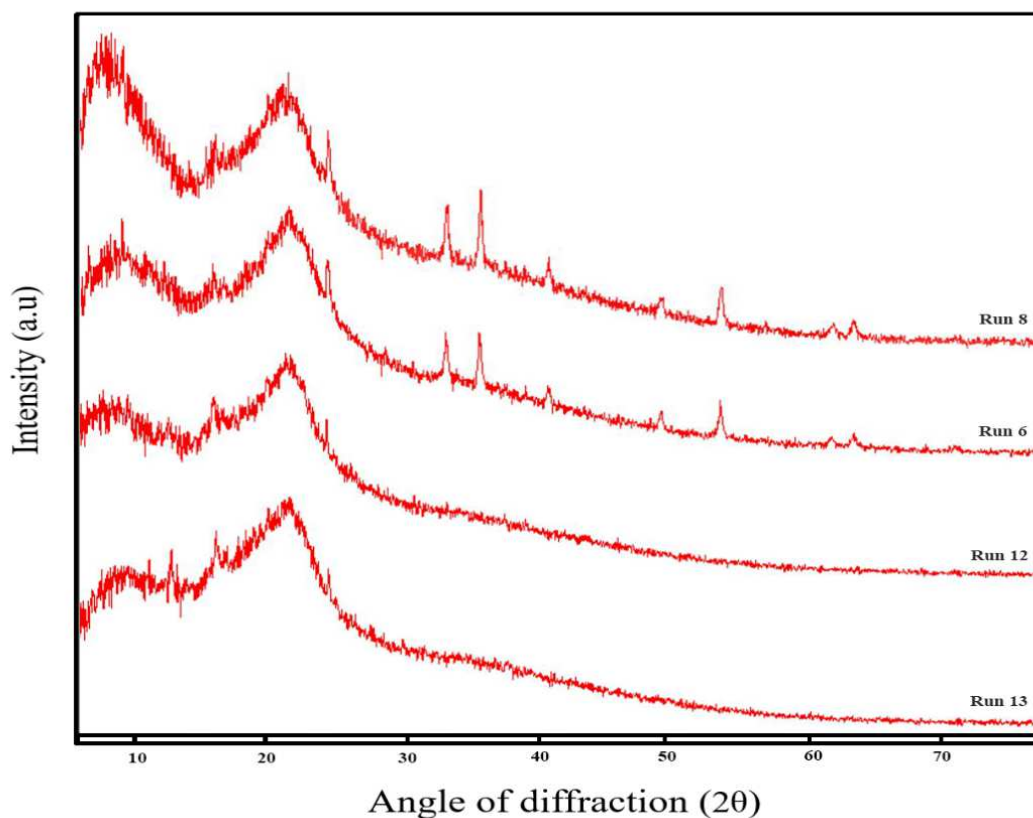
454 and nanoparticles was compared with the control sample (RNU 13) using the XRD test,

455 which is shown in Fig. 13. The XRD spectrum of the film indicated that the films in 2θ of

456 12.3, 15.8, and 24.5 have sharp peaks, indicating the existence of crystalline structures in
457 these films. Besides, those peaks with relatively broad heads in 2θ of 8 and 12, indicate the
458 existence of an amorphous structure or irregularity in the film .

459 By adding gum Arabic in sample 12, the peak of $2\theta=12.3$ was removed while the peak height
460 of $2\theta=15.8$ was decreased. Meanwhile, the head of peak $2\theta=8$ was also relatively wider. All
461 these changes including reduced crystalline structure, the presence of crystals, and the
462 increased amorphous structure in the film structure are caused by gum Arabic, as compared
463 to the control sample. In the XRD spectrum of samples 6 with the highest percentage of
464 nanoparticles and Arab gum, some new peaks in 2θ of 33.7, 36.2, 41.6, 50.3, 58.9, 63.5, and
465 65 are created. All these sharp peaks indicate crystallization and the formation of new
466 crystals in sample 6, as compared to sample 13 as a result of the crystallization of
467 nanoparticles added to the film structure.

468 In sample 8 with the highest percentage of gum and nanoparticles, in comparison with sample
469 13, a displacement was created in the peak from $2\theta=8$ to $2\theta=7$, such that the height of this
470 peak was increased, indicating an increase in the crystallization degree of this sample, as
471 compared to sample 13. In comparison with sample 6, a shift was created in sample 8 from
472 $2\theta=58.9$ to $2\theta=54.8$, in which the height of the peak was increased. Furthermore, in 2θ of
473 33.7, 36.2, and 41.6, the height of the peaks was increased, while at $2\theta=50.3$, the height of the
474 peak was decreased. Overall, the crystallization degree of sample 8 was more than other
475 tested samples, indicating that the addition of gum Arabic and nanoparticles simultaneously
476 caused new crystals, finally increasing the crystallization degree of the film .



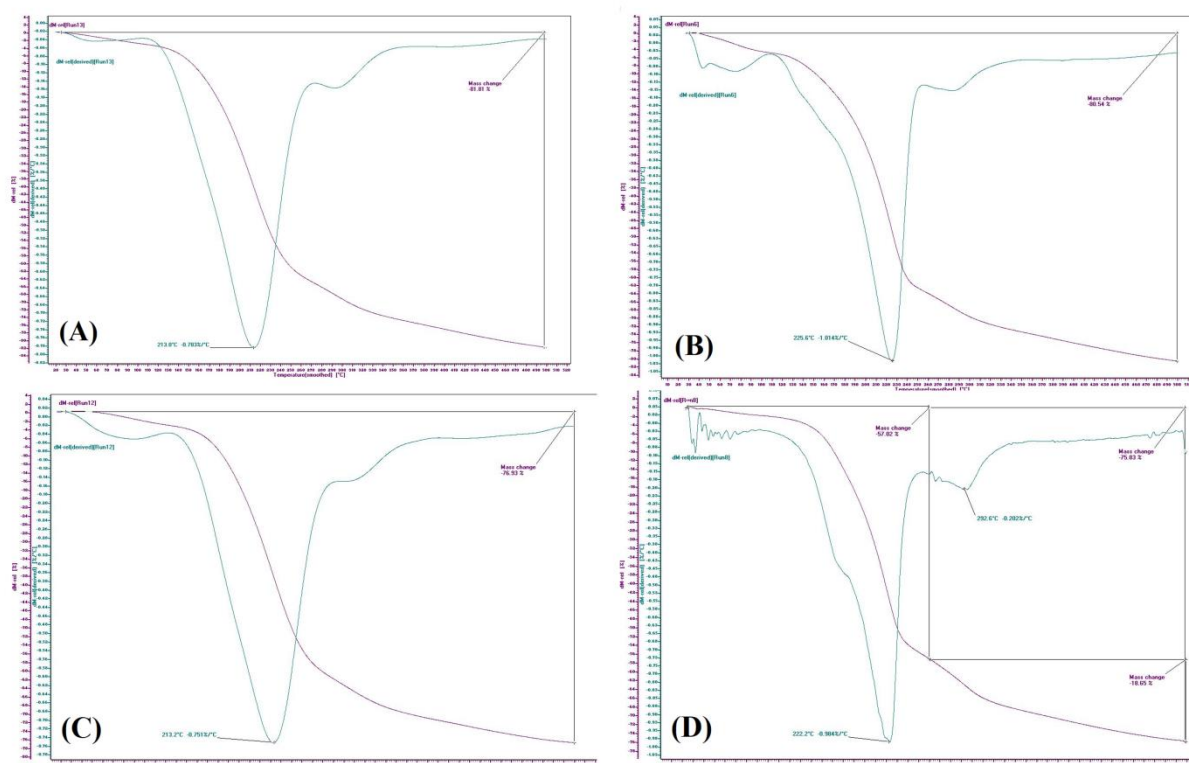
477
 478 **Fig. 13:** The XRD curve (RUN 13) curve OPP, (Run 6) OPP / Cr₂O₃, (RUN12) OPP /
 479 AG, and (RUN 8) OPP / Cr₂O₃ / AG

480
 481 **Thermogravimetric analysis (TGA) change test**

482 TGA analysis is employed to investigate the thermal stability of the films. TGA and DTG
 483 thermal diagrams are provided in Fig. 14. In all film samples, the initial weight drop was
 484 observed at 70-120 °C because of the evaporation of moisture from the surface of the films
 485 [38]. The next weight drop was observed at around 150-250 °C because of the thermal
 486 decomposition of polymer and glycerol evaporation used as a plasticizer [46].

487 In this regard, similar results were proposed by Slavutsky et al. [47] for the film based on
 488 Montmorillonite nanoparticles and BREA gum. The maximum decomposition temperature
 489 specified from the temperature peak of the DTG curve is 213° C for the control and film
 490 samples containing 5% gum Arabic, whereas it is 225 °C for film samples containing 3% of

491 the chromium oxidized nanoparticles, gum, and nanoparticles. As can be observed, by adding
 492 the nanoparticles, the maximum decomposition temperature increases, as compared to the
 493 film samples without the nanoparticles. Furthermore, these results indicate that the thermal
 494 stability of orange peel film increases by adding the Cr₂O₃ NPs. Such behavior is likely due
 495 to the increased bending in the path of gas emissions as well as the restriction of oxygen and
 496 gases emission from the pyrolysis [47]. Oun and Rhim [39] proposed similar results reporting
 497 that the addition of zinc oxide nanoparticles to Carrageenans-based films increased the
 498 stability of films.



499
 500 **Fig. 14:** The TGA curve of (A) OPP, (B) OPP / Cr₂O₃, (C) OPP / AG and (D) OPP / Cr₂O₃ /
 501 AG

502
 503 **Investigating antimicrobial properties of films**

504 The disk diffusion method was employed to specify the antimicrobial properties of gum and
 505 Cr₂O₃ NPs. In this technique, a piece of antimicrobial film is placed in a solid culture medium

506 containing the target microorganisms. After incubation at a specific temperature, the bright
 507 halo around the film represents the emission of the antimicrobial agent from the film and thus
 508 inhibition of the target microorganisms' growth. The disk diffusion method simulates
 509 packaging the food, indicating the performance of the film in contact with the contaminated
 510 surfaces as well as the immigration of the antimicrobial agent from the film to food [48].
 511 The results of antimicrobial activity of gum and nanoparticles samples are illustrated in
 512 comparison with the control sample on the gram-positive bacteria of *S. aureus* and gram-
 513 negative bacteria of *E. coli* in Fig. 15. As can be observed, the control sample does not show
 514 the antimicrobial properties against both bacteria, and the halo is not observed around the
 515 film disk. Based on the obtained image, with the addition of gum and nanoparticles, the
 516 growth halo was observed around the films, indicating the release of antimicrobial agents.
 517 Nevertheless, as seen, the most halo was created in sample 8. However, there was no
 518 synergistic effect of gum and nanoparticles to destruct the tested microorganisms .

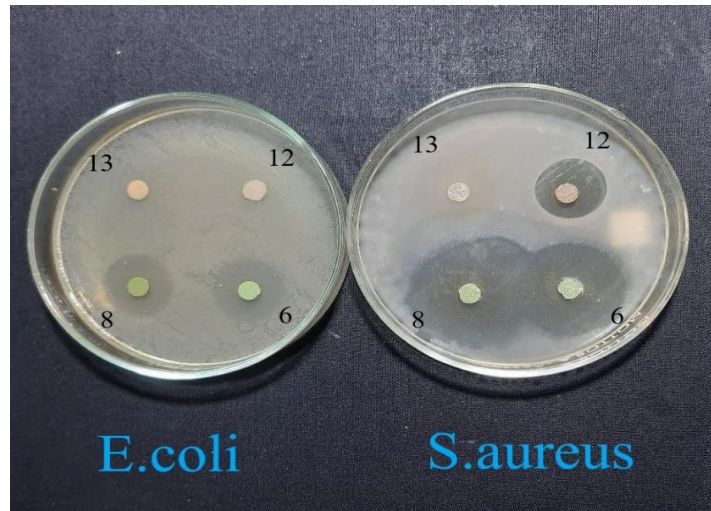
519 **Table 2:** The results of the microbial test of films based on orange peel and gum Arabic

Sample	Diameter of non-growth area (mm)	
	<i>Staphylococcus aureus</i>	<i>Escherichia coli</i>
OPP	0 ^a	0 ^a
OPP /AG	19.59 ±1.24 ^b	0 ^a
OPP /Cr ₂ O ₃	33.03 ±1.34 ^c	20.42 ±1.64 ^b
OPP /Cr ₂ O ₃ /AG	36.30 ± 2.30 ^c	18.99 ±1.02 ^b

520 Different letters in each column indicate the significance at the level of p <0.05 .

521
 522 Moreover, as seen, adding gum alone did not have a specific antimicrobial effect on the
 523 gram-negative bacteria of *E. coli*, which can be due to the presence of liposaccharide walls
 524 around the Peptidoglycan wall of gram-negative bacteria resulting in more bacterial

525 resistance against the antibacterial agents [49]. The destruction of microorganisms due to the
526 addition of nanoparticles can be associated with the leakage of intracellular materials by the
527 holes generated on the cell wall. These holes are formed by oxidation of wall liposaccharides
528 of cells owing to the nanoparticles-caused changes and differences .



529

530 **Fig. 15:** The images of antimicrobial properties of films (RUN 13) OPP, (RUN 6) OPP/
531 Cr_2O_3 , (RUN12) OPP/ AG, and (RUN 8) OPP/ Cr_2O_3 / AG

532

533 **Conclusion**

534 In this paper, OPP was utilized as an available, abundant, and cheap substance, compared to
535 gum Arabic to prepare the edible films. Examining these films indicated that they had
536 mechanical properties, inhibition, and good water solubility. The results revealed that the film
537 solubility decreased by increasing the percentage of gum and Cr_2O_3 NPs . Furthermore, by
538 adding gum Arabic and nanoparticles, the tensile strength parameter had a significant
539 increase, as compared to the control sample, which could be associated with the creation of
540 appropriate interactions between film matrix and additive materials (such as gum Arabic and
541 Cr_2O_3 NPs). Besides, the creation of new hydrogen bonding increased the parameter.
542 Moreover, the transparency of the films increased significantly by increasing the percentage
543 of gum. The antimicrobial properties of the films increased significantly by increasing the

544 nanoparticle percentage. Furthermore, the results of X-ray diffraction analysis confirmed a
545 decreased crystalline structure and increased Amorphous structure because of the addition of
546 gum Arabic .

547

548 **Refernces**

- 549 [1] Gholam-Zhiyan, A., Amiri, S., Rezazadeh-Bari, M., & Pirs, S. (2021). Stability of
550 *Bacillus coagulans* IBRC-M 10807 and *Lactobacillus plantarum* PTCC 1058 in Milk
551 Proteins Concentrate (MPC)-Based Edible Film. *Journal of Packaging Technology*
552 *and Research*, 5(1), 11-22.
- 553 [2] Jabraili, A., Pirs, S., Pirouzifard, M. K., & Amiri, S. (2021). Biodegradable
554 nanocomposite film based on gluten/silica/calcium chloride: physicochemical
555 properties and bioactive compounds extraction capacity. *Journal of Polymers and the*
556 *Environment*, 1-15.
- 557 [3] Alizadeh, N., Ataei, A. A., & Pirs, S. (2015). Nanostructured conducting polypyrrole
558 film prepared by chemical vapor deposition on the interdigital electrodes at room
559 temperature under atmospheric condition and its application as gas sensor. *Journal of*
560 *the Iranian Chemical Society*, 12(9), 1585-1594.
- 561 [4] Gennadios, A. (Ed.). (2002). *Protein-based films and coatings*. CRC press.
- 562 [5] Giménez, B., Gómez-Estaca, J., Alemán, A., Gómez-Guillén, M. C., & Montero, M. P.
563 (2009). Improvement of the antioxidant properties of squid skin gelatin films by the
564 addition of hydrolysates from squid gelatin. *Food Hydrocolloids*, 23(5), 1322-1327.
- 565 [6] Pirs, S., & Aghbolagh Sharifi, K. (2020). A review of the applications of bioproteins in
566 the preparation of biodegradable films and polymers. *Journal of Chemistry*
567 *Letters*, 1(2), 47-58.
- 568 [7] Labuza, T. P., & Breene, W. M. (1989). Applications of “active packaging” for
569 improvement of shelf-life and nutritional quality of fresh and extended shelf-life
570 foods 1. *Journal of Food Processing and Preservation*, 13(1), 1-69.
- 571 [8] Amiri, S., Saray, F. R., Rezazad-Bari, L., & Pirs, S. (2021). Optimization of extraction
572 and characterization of physicochemical, structural, thermal, and antioxidant
573 properties of mucilage from Hollyhock’s root: a functional
574 heteropolysaccharide. *Journal of Food Measurement and Characterization*, 15(3),
575 2889-2903.
- 576 [9] Verbeken, D., Dierckx, S., & Dewettinck, K. (2003). Exudate gums: occurrence,
577 production, and applications. *Applied Microbiology and Biotechnology*, 63(1), 10-21.
- 578 [10] Sciarini, L. S., Maldonado, F., Ribotta, P. D., Pérez, G. T., & León, A. E. (2009).
579 Chemical composition and functional properties of *Gleditsia triacanthos* gum. *Food*
580 *Hydrocolloids*, 23(2), 306-313.
- 581 [11] Xu, T., Gao, C., Feng, X., Huang, M., Yang, Y., Shen, X., & Tang, X. (2019). Cinnamon
582 and clove essential oils to improve physical, thermal and antimicrobial properties of
583 chitosan-gum arabic polyelectrolyte complexed films. *Carbohydrate polymers*, 217,
584 116-125.

- 585 [12] Shanthilal, J., & Bhattacharya, S. (2017). Frying of rice flour dough strands containing
586 gum Arabic: texture, sensory attributes and microstructure of products. *Journal of*
587 *Food Science and Technology*, 54(5), 1293-1303.
- 588 [13] Manthey, J. A., & Grohmann, K. (2001). Phenols in citrus peel byproducts.
589 Concentrations of hydroxycinnamates and polymethoxylated flavones in citrus peel
590 molasses. *Journal of Agricultural and Food Chemistry*, 49(7), 3268-3273.
- 591 [14] Bocco, A., Cuvelier, M. E., Richard, H., & Berset, C. (1998). Antioxidant activity and
592 phenolic composition of citrus peel and seed extracts. *Journal of Agricultural and*
593 *Food Chemistry*, 46(6), 2123-2129.
- 594 [15] Mascolo, C., Marrone, R., Palma, A., & Palma, G. (2013). Nutritional value of fish
595 species. *Journal of Nutritional Ecology and Food Research*, 1(3), 219-225.
- 596 [16] Pirsá, S., Abdolsattari, P., Peighambaroust, S. J., Fasihnia, S. H., & Peighambaroust,
597 S. H. (2020). Investigating microbial properties of traditional Iranian white cheese
598 packed in active LDPE films incorporating metallic and organoclay
599 nanoparticles. *Chemical Review and Letters*, 3(4), 168-174.
- 600 [17] Pirsá, S., Farshchi, E., & Roufegarinejad, L. (2020). Antioxidant/antimicrobial film
601 based on carboxymethyl cellulose/gelatin/TiO₂-Ag nano-composite. *Journal of*
602 *Polymers and the Environment*, 28(12), 3154-3163.
- 603 [18] Hassannia-Kolae, M., Khodaiyan, F., Pourahmad, R., & Shahabi-Ghahfarrokhi, I.
604 (2016). Development of ecofriendly bionanocomposite: Whey protein isolate/pullulan
605 films with nano-SiO₂. *International Journal of Biological Macromolecules*, 86, 139-
606 144.
- 607 [19] Ghamari, M. A., Amiri, S., Rezazadeh-Bari, M., & Rezazad-Bari, L. (2021). Physical,
608 mechanical, and antimicrobial properties of active edible film based on milk proteins
609 incorporated with *Nigella sativa* essential oil. *Polymer Bulletin*, 1-21.
- 610 [20] Zhu, J. Y., Tang, C. H., Yin, S. W., & Yang, X. Q. (2018). Development and
611 characterization of novel antimicrobial bilayer films based on Polylactic acid
612 (PLA)/Pickering emulsions. *Carbohydrate Polymers*, 181, 727-735.
- 613 [21] Jouki, M., Khazaei, N., Ghasemlou, M., & HadiNezhad, M. (2013). Effect of glycerol
614 concentration on edible film production from cress seed carbohydrate
615 gum. *Carbohydrate Polymers*, 96(1), 39-46.
- 616 [22] Asdagh, A., & Pirsá, S. (2020). Bacterial and oxidative control of local butter with
617 smart/active film based on pectin/nanoclay/*Carum copticum* essential oils/ β -
618 carotene. *International Journal of Biological Macromolecules*, 165, 156-168.
- 619 [23] Salas-Valero, L. M., Tapia-Blácido, D. R., & Menegalli, F. C. (2015). Biofilms based on
620 canihua flour (*Chenopodium Pallidicaule*): Design and characterization. *Química*
621 *Nova*, 38(1), 14-21.
- 622 [24] Bazargani-Gilani, B., Aliakbarlu, J., & Tajik, H. (2015). Effect of pomegranate juice
623 dipping and chitosan coating enriched with *Zataria multiflora Boiss* essential oil on
624 the shelf-life of chicken meat during refrigerated storage. *Innovative Food Science &*
625 *Emerging Technologies*, 29, 280-287.
- 626 [25] Bahrami, A., Mokarram, R. R., Khiabani, M. S., Ghanbarzadeh, B., & Salehi, R. (2019).
627 Physico-mechanical and antimicrobial properties of tragacanth/hydroxypropyl
628 methylcellulose/beeswax edible films reinforced with silver nanoparticles.
629 *International Journal of Biological Macromolecules*, 129, 1103-1112.

- 630 [26] Oleyaei, S. A., Zahedi, Y., Ghanbarzadeh, B., & Moayedi, A. A. (2016). Modification of
631 physicochemical and thermal properties of starch films by incorporation of TiO₂
632 nanoparticles. *International Journal of Biological Macromolecules*, 89, 256-264.
- 633 [27] Li, L. H., Deng, J. C., Deng, H. R., Liu, Z. L., & Li, X. L. (2010). Preparation,
634 characterization and antimicrobial activities of chitosan/Ag/ZnO blend
635 films. *Chemical Engineering Journal*, 160(1), 378-382.
- 636 [28] Pirsa, S. (2020). Biodegradable film based on pectin/Nano-clay/methylene blue:
637 Structural and physical properties and sensing ability for measurement of vitamin C.
638 *International Journal of Biological Macromolecules*, 163, 666-675.
- 639 [29] Rezaei, M., Pirsa, S., & Chavoshizadeh, S. (2019). Photocatalytic/antimicrobial active
640 film based on wheat gluten/ZnO nanoparticles. *Journal of Inorganic and
641 Organometallic Polymers and Materials*, 1-12.
- 642 [30] Sui, C., Zhang, W., Ye, F., Liu, X., & Yu, G. (2016). Preparation, physical, and
643 mechanical properties of soy protein isolate/guar gum composite films prepared by
644 solution casting. *Journal of Applied Polymer Science*, 133(18).
- 645 [31] Khoirunnisa, A. R., Joni, I. M., Panatarani, C., Rochima, E., & Praseptiangga, D. (2018,
646 February). UV-screening, transparency and water barrier properties of semi refined
647 iota carrageenan packaging film incorporated with ZnO nanoparticles. In AIP
648 Conference Proceedings (Vol. 1927, No. 1, p. 030041). AIP Publishing LLC.
- 649 [32] Tunç, S., & Duman, O. (2010). Preparation and characterization of biodegradable methyl
650 cellulose/montmorillonite nanocomposite films. *Applied Clay Science*, 48(3), 414-
651 424.
- 652 [33] Baek, S. K., & Song, K. B. (2018). Development of Gracilaria vermiculophylla extract
653 films containing zinc oxide nanoparticles and their application in smoked salmon
654 packaging. *LWT*, 89, 269-275.
- 655 [34] Anaya-Esparza, L. M., Ruvalcaba-Gómez, J. M., Maytorena-Verdugo, C. I., González-
656 Silva, N., Romero-Toledo, R., Aguilera-Aguirre, S., & Pérez-Larios, A. (2020).
657 Chitosan-TiO₂: A Versatile Hybrid Composite. *Materials*, 13(4), 811.
- 658 [35] Asdagh, A., Sani, I. K., Pirsa, S., Amiri, S., Shariatifar, N., Eghbaljoo-
659 Gharegheshlaghi, H., ... & Taniyan, A. (2021). Production and characterization of
660 nanocomposite film based on whey protein isolated/copper oxide nanoparticles
661 containing coconut essential oil and paprika extract. *Journal of Polymers and the
662 Environment*, 29(1), 335-349.
- 663 [36] He, Q., Zhang, Y., Cai, X., & Wang, S. (2016). Fabrication of gelatin-TiO₂
664 nanocomposite film and its structural, antibacterial and physical
665 properties. *International Journal of Biological Macromolecules*, 84, 153-160.
- 666 [37] Farshchi, E., Pirsa, S., Roufegarinejad, L., Alizadeh, M., & Rezazad, M. (2019).
667 Photocatalytic/biodegradable film based on carboxymethyl cellulose, modified by
668 gelatin and TiO₂-Ag nanoparticles. *Carbohydrate Polymers*, 216, 189-196.
- 669 [38] Kanmani, P., & Rhim, J. W. (2014). Physicochemical properties of gelatin/silver
670 nanoparticle antimicrobial composite films. *Food Chemistry*, 148, 162-169.
- 671 [39] Oun, A. A., & Rhim, J. W. (2017). Carrageenan-based hydrogels and films: Effect of
672 ZnO and CuO nanoparticles on the physical, mechanical, and antimicrobial
673 properties. *Food Hydrocolloids*, 67, 45-53.
- 674 [40] Balasubramanian, R., Kim, S. S., Lee, J., & Lee, J. (2019). Effect of TiO₂ on highly
675 elastic, stretchable UV protective nanocomposite films formed by using a

676 combination of k-Carrageenan, xanthan gum and gellan gum. *International Journal of*
677 *Biological Macromolecules*, 123, 1020-1027.

678 [41] Martins, J. T., Bourbon, A. I., Pinheiro, A. C., Souza, B. W., Cerqueira, M. A., &
679 Vicente, A. A. (2013). Biocomposite films based on κ -carrageenan/locust bean gum
680 blends and clays: physical and antimicrobial properties. *Food and Bioprocess*
681 *Technology*, 6(8), 2081-2092.

682 [42] Piñeros-Hernandez, D., Medina-Jaramillo, C., López-Córdoba, A., & Goyanes, S.
683 (2017). Edible cassava starch films carrying rosemary antioxidant extracts for
684 potential use as active food packaging. *Food Hydrocolloids*, 63, 488-495.

685 [43] Choo, K., Ching, Y. C., Chuah, C. H., Julai, S., & Liou, N. S. (2016). Preparation and
686 characterization of polyvinyl alcohol-chitosan composite films reinforced with
687 cellulose nanofiber. *Materials*, 9(8), 644.

688 [44] Li, H., Pu, Y., Kumar, R., Ragauskas, A. J., & Wyman, C. E. (2014). Investigation of
689 lignin deposition on cellulose during hydrothermal pretreatment, its effect on
690 cellulose hydrolysis, and underlying mechanisms. *Biotechnology and*
691 *Bioengineering*, 111(3), 485-492.

692 [45] Lozano-Navarro, J. I., Díaz-Zavala, N. P., Velasco-Santos, C., Melo-Banda, J. A.,
693 Páramo-García, U., Paraguay-Delgado, F., ... & Zapién-Castillo, S. (2018). Chitosan-
694 starch films with natural extracts: Physical, chemical, morphological and thermal
695 properties. *Materials*, 11(1), 120.

696 [46] Shankar, S., Teng, X., & Rhim, J. W. (2014). Properties and characterization of
697 agar/CuNP bionanocomposite films prepared with different copper salts and reducing
698 agents. *Carbohydrate Polymers*, 114, 484-492.

699 [47] Slavutsky, A. M., Bertuzzi, M. A., Armada, M., García, M. G., & Ochoa, N. A. (2014).
700 Preparation and characterization of montmorillonite/brea gum nanocomposites films.
701 *Food Hydrocolloids*, 35, 270-278.

702 [48] Genskowsky, E., Puente, L. A., Pérez-Álvarez, J. A., Fernandez-Lopez, J., Muñoz, L.
703 A., & Viuda-Martos, M. (2015). Assessment of antibacterial and antioxidant
704 properties of chitosan edible films incorporated with maqui berry (*Aristotelia*
705 *chilensis*). *LWT-Food Science and Technology*, 64(2), 1057-1062.

706 [49] Burt, S. (2004). Essential oils: their antibacterial properties and potential applications in
707 foods—a review. *International Journal of Food Microbiology*, 94(3), 223-253.

708
709
710